Performance of IR-HARQ-based RC-LDPC Code Extension in Optical Satellite Systems

Cuong T. Nguyen, Hoang D. Le, and Anh T. Pham
Computer Communications Laboratory, The University of Aizu, Aizuwakamatsu 965-8580, Japan

***Abstract*—This paper studies the link-layer error-control solutions for low Earth orbit (LEO) satellite-based free-space optical (FSO) communications. Specifically, we address the design of low-density parity check (LDPC) codes for incremental redundancy (IR) hybrid automatic repeat request (HARQ) protocols. To facilitate the IR-HARQ operation, a rate-compatible (RC)-LDPC code family constructed by the code extension method is used. Performance metrics, including goodput and energy efficiency, are investigated. Simulation results confirm the effectiveness of our proposed design compared to existing solutions over the state-of-the-art. The results also support the proper selection of the LEO satellite's transmitted powers based on the trade-off between goodput and energy efficiency.**

***Index Terms*—Free-space optics (FSO), hybrid automatic repeat request (HARQ), low-density parity check (LDPC) codes, low earth orbits (LEO) satellite**

I. Introduction

In the vision of future sixth-generation (6G) wireless communications, the Internet of Things (IoT) is expected to enable a wide range of applications, such as the Internet of Vehicles (IoV), intelligent agriculture, and healthcare IoT [1]. The existing terrestrial infrastructure supporting IoT may not meet the stringent requirements for global coverage and high network capacity. Recent years have witnessed the rapid development of low-Earth orbit (LEO) satellites forming constellation networks to provide global Internet from space, e.g., in many projects of SpaceX's Starlink, OneWeb, and Telesat [2]. LEO satellites offer low latency and less power consumption compared to other types of satellites [3]. In addition, free-space optical (FSO) technology has established its reputation for delivering extremely high-speed data services thanks to its broad license-free bandwidth [4]. Therefore, LEO satellite-based FSO communication is a potential candidate for many application services toward 6G networks, as shown in Fig. 1.

The uncertainty of atmospheric channels, especially the signal fading due to atmospheric turbulence, poses various issues in designing satellite-based FSO systems [5]. A feasible solution to tackle this issue is the use of hybrid automatic repeat request (HARQ) protocols, which integrate automatic repeat requests (ARQ) and error correction codes (ECC) [6]. The design and performance evaluation of HARQ protocols have been recently investigated in LEO satellite-based FSO systems [2], [6]–[8]. Notably, the design of cooperative incremental redundancy (IR) HARQ, considering the sliding window ARQ and the punctured Reed-Solomon (RS) code, was introduced in [2], [7]. The performance of IR-HARQ based on the rate-compatible punctured convolutional (RCPC) code family with rate adaptation was analyzed in [6]. Most recently, the authors in [8] formulated the power optimization problem for LEO satellite-based FSO systems using different HARQ schemes. These studies confirmed the effectiveness of IR-HARQ over the time-varying FSO channels thanks to transmissions of incremental parity bits to correct erroneous frames.

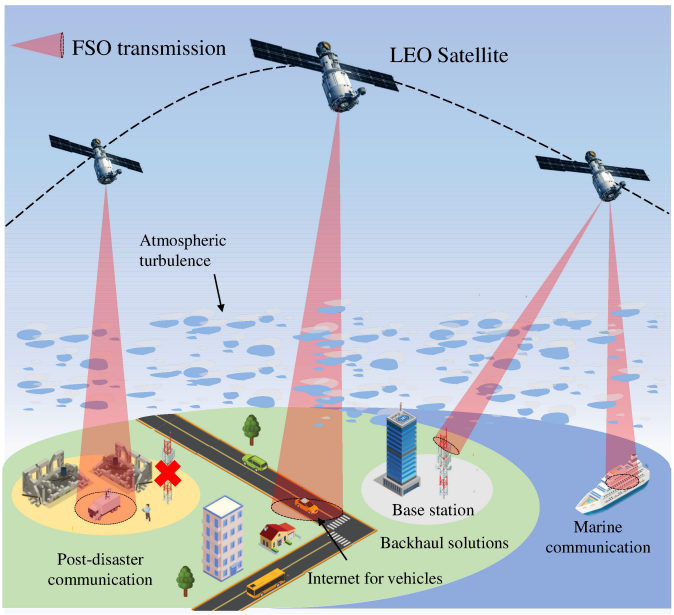

Fig. 1. An example of LEO satellite-based FSO systems supporting various applications.

The above-mentioned studies focused on punctured codes of either RS or convolutional codes for the IR-HARQ design. Nevertheless, the FSO channel coherence time is typically in the order of milliseconds, and long data frames are preferred for Gbps-rate transmissions [6]. Such long codewords result in exponentially increasing complexity in the Viterbi decoder of the convolutional codes [9]. Additionally, while long RS codes implemented on a large-size Galois field have been considered [10], it is still not feasible due to the high complexity. A viable solution is the employment of low-density parity check (LDPC) code for the HARQ design. The LDPC codes, which is a type of linear block code, have received tremendous attention thanks to low decoding complexity and close-to-capacity performance [11]. To facilitate the operation of IR-HARQ

protocols, the rate-compatible (RC)-LDPC code family, which is a set of nested LDPC code rates, is employed. To obtain such an RC-LDPC code family, there are two popular approaches, i.e., puncturing and code extension. The puncturing method, which achieves higher code rates by removing coded bits from a lower mother code rate, may suffer from painstaking optimization and performance degradation at higher code rates [11]. At the same time, the code extension method constructs the RC-LDPC code family by extending a parity check matrix of high-rate code to obtain the lower code rates, which can curtail the drawback of the puncturing method [11]. However, the design of the IR-HARQ-based RC-LDPC code extension has not been studied in the literature on LEO satellite-based FSO systems.

This paper, therefore, aims to address the design and performance evaluation of IR-HARQ-based RC-LDPC code extension in LEO satellite-based FSO systems. The sliding window mechanism is employed for IR-HARQ protocols. Additionally, the HARQ's window size is designed by a burst size to effectively facilitate the operation of the IR-HARQ protocol. Performance metrics, including goodput and energy efficiency, are investigated over turbulence-induced fading channels. Simulation results highlight the effectiveness of our proposed solution and discuss a proper selection of the system's parameters.

II. System and Channel Models

A. System Description

As illustrated in Fig. 1, we consider an FSO transmission from an LEO satellite to a ground station. The IR-HARQ protocol, which combines the sliding window ARQ and RC-LDPC code, is employed at the link layer to guarantee the system's reliability. The RC-LDPC-based code extension is used to correct the corrupted frames using the iterative belief propagation (BP) algorithm. In addition, the sliding window ARQ scheme is for the retransmission of additional redundancies for erroneous frames, which are uncorrected by the RC-LDPC code. For the sake of simplicity, feedback signals, i.e., ACK and NAK, are supposed to be error-free.

On the other hand, we consider a fixed-size time-slot structure for data transmission. Each time slot accommodates a burst transmission of multiple data/redundancy frames and its feedback signal. The burst duration is designed to be shorter than the FSO channel coherence time so that frames in a burst are assumed to experience the same channel condition. The time slot duration t_{slot} can be written as $t_{\text{slot}} = t_{\text{trans}} + 2t_{\text{prop}}$, where t_{prop} is the propagation delay, and $t_{\text{trans}} = N_{\text{burst}}/R_{\text{b}}$, where N_{burst} and R_{b} are the number of bits per burst and data bit rate, respectively. It is worth noting that different sizes of a given frame, which is for initial transmission and retransmissions, can be used. This results in size-varying burst transmissions. To keep the fixed-size bursts, the transmitter fills up the burst with new transmissions and zero paddings after sending all incremental retransmissions.

We consider the intensity modulation/direct detection (IM/DD) with on-off keying (OOK) modulation for the system. Thus, the received electrical signal is given as [12]

$$y = \Re h x + n, \tag{1}$$

where $\Re$ is the detector responsivity, h is the channel fading coefficient considered to be constant over a burst transmission, $x \in \{x_0 = 0, x_1 = 2P_{\text{t}}\}$ is the transmitted intensity with average transmitted optical power P_{t}, and n denotes the additive white Gaussian noise (AWGN) with zero mean and variance σ_{n}^2. The instantaneous electrical signal-to-noise ratio (SNR) at the receiver thus can be expressed as

$$\gamma = \frac{\bar{\gamma} h^2}{\mathbb{E}\left[h^2\right]} = \frac{2\left(\Re P_{\text{t}} h\right)^2}{\sigma_{\text{n}}^2}, \tag{2}$$

where $\bar{\gamma} = \frac{2(\Re P_{\text{t}})^2}{\sigma_{\text{n}}^2}\mathbb{E}\left[h^2\right]$ is the average electrical SNR.

B. FSO Channel Model

The channel fading coefficient h consists of three factors, i.e. atmospheric attenuation h_{l}, atmospheric turbulence h_{a}, beam spreading loss h_{p} and can be written as $h = h_{\text{l}} h_{\text{a}} h_{\text{p}}$. Details of these factors are as follows.

1) Atmospheric Attenuation: The atmospheric attenuation is deterministic, which is calculated by Beer Lambert's law as

$$h_{\text{l}} = \exp\left(-\sigma L\right), \tag{3}$$

where σ is the attenuation coefficient and can be expressed as the function of the visibility V and the optical wavelength λ in [4, (4)]; L is the communication distance and can be computed as $L = (H_{\text{s}} - H_{\text{r}})\sec(\xi)$ where H_{s} and H_{r} are respectively the altitude of the satellite and the ground station, ξ is the zenith angle, $\sec(.)$ is the secant function.

2) Atmospheric Turbulence Fading: For the atmospheric turbulence fading, we consider the Gamma-Gamma distributed random variable to model a wide range of turbulence conditions, from weak to strong [5]. Therefore, the probability density function of the fading coefficient h_{a} is given as

$$f_{h_{\text{a}}}(h_{\text{a}}) = \frac{2(\alpha\beta)^{\frac{\alpha+\beta}{2}}}{\Gamma(\alpha)\Gamma(\beta)} h_{\text{a}}^{\frac{\alpha+\beta}{2}-1} K_{\alpha-\beta}\left(2\sqrt{\alpha\beta h_{\text{a}}}\right), \tag{4}$$

where $\Gamma(.)$ is the Gamma function, $K_{\alpha-\beta}(.)$ is the modified Bessel function of the second kind of order $\alpha - \beta$. The shaping parameters α and β are determined as functions of the Rytov variance σ_{R}^2 [5]. Under the assumption of plane wave propagation, the Rytov variance is written as

$$\sigma_{\text{R}}^2 = 2.25 k_{\text{wave}}^{7/6} \sec^{11/6}(\xi) \int_{H_{\text{r}}}^{H_{\text{a}}} C_n^2(h)\,(h - H_{\text{r}})^{5/6}\,\mathrm{d}h, \tag{5}$$

where $k_{\text{wave}} = 2\pi/\lambda$ is the optical wave number, H_{a} is the atmospheric altitude. Moreover, $C_n^2(h)$ is the altitude-dependent refractive index structure coefficient and can be modeled by the Hufnagel-Valley model as $C_n^2(h) = 0.00594\left(\frac{w_{\text{wind}}}{27}\right)^2\left(10^{-5}h\right)^{10}\exp\left(-\frac{h}{1000}\right) + 2.7 \times 10^{-16}\exp\left(-\frac{h}{1500}\right) + C_n^2(0)\exp\left(-\frac{h}{100}\right)$, where $C_n^2(0)$ is the ground-level turbulence , and w_{wind} is root-mean-squared (rms) wind speed [5].

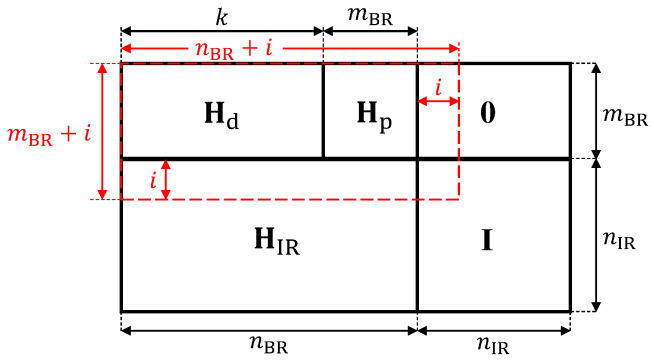

Fig. 2. Structure diagram of an RC-LDPC code family's parity check matrix derived by code extension.

3) Beam-spreading Loss: We consider a Gaussian beam profile with the perfect tracking system [3]. As a result, the fraction of collected power at the receiver's circular detector can be approximated as [12]

$$h_{\mathrm{p}} \approx A_0 \exp\left(-\frac{2\rho^2}{w_{L_{\mathrm{eq}}}^2}\right), \tag{6}$$

where ρ is the radial displacement, $A_0 = [\mathrm{erf}(v)]^2$ is the fraction of the collected power at $\rho = 0$ with $v = (\sqrt{\pi} r_{\mathrm{a}}) / (\sqrt{2} w_{L,\mathrm{eff}})$, $\mathrm{erf}(.)$ is the error function, r_{a} is the receiver aperture radius, $w_{L_{\mathrm{eq}}}$ is the equivalent beam width and can be expressed as$w_{L_{\mathrm{eq}}}^2 = w_{L,\mathrm{eff}}^2 \frac{\sqrt{\pi}\mathrm{erf}(v)}{2v\exp(-v^2)}$. Moreover, $w_{L,\mathrm{eff}}$ is the effective beam width in the presence of optical turbulence at the communication distance L and can be calculated as $w_{L,\mathrm{eff}} = w_{\mathrm{L}}\sqrt{1+G_{\mathrm{d}}}$ where G_{d} can be found in [13, (16)]. w_{L} is the diffractive beam radius at distance L and is written as $w_{\mathrm{L}} = w_0\sqrt{\left(1-\frac{L}{F_0}\right)^2 + \left(\frac{2L}{k_{\mathrm{wave}} w_0^2}\right)^2}$, where $w_0 = \frac{\pi}{\lambda\theta}$ and F_0 are, respectively, the beam radius and phase font radius of curvature at the transmitter output aperture, θ is the divergence half-angle.

III. IR-HARQ-based RC-LDPC Code Extension

This section focuses on the IR-HARQ-based RC-LDPC Code Extension. First, we introduce the RC-LDPC code extension. Then, the operation of IR-HARQ-based RC-LDPC Code Extension with FSO burst transmission is described.

A. Rate-compatible (RC) LDPC Code Extension

RC-LDPC codes are employed to correct erroneous frames using the LDPC encoder/decoder. They allow the encoder/decoder pair to adjust different code rates without changing their basic structure. All coded bits of low-rate RC-LDPC codes are extended from a high-rate code (a base rate) based on the extension of its parity check matrix. Fig. 2 illustrates the structure diagram of an RC-LDPC code family's parity check matrix derived by code extension. The matrix includes five sub-matrices where $\mathbf{H}_{\mathrm{d}}$ is a $m_{\mathrm{BR}} \times k$ sub-matrix corresponding to data bits of the base rate, $\mathbf{H}_{\mathrm{p}}$ is a $m_{\mathrm{BR}} \times m_{\mathrm{BR}}$ sub-matrix corresponding to the parity bits of the base rate, $\mathbf{H}_{\mathrm{IR}}$ is a $n_{\mathrm{IR}} \times n_{\mathrm{BR}}$ sub-matrix corresponding to the extension part, $\mathbf{I}$ is an identity matrix, and $\mathbf{0}$ is a zero sub-matrix. Here, we consider the quasi-cyclic LDPC code, whose parity matrix is in the circulant form, i.e., $\mathbf{H}_{\mathrm{d}}$, $\mathbf{H}_{\mathrm{p}}$, and $\mathbf{H}_{\mathrm{IR}}$, [14]. The encoder/decoder of such quasi-LDPC codes can be efficiently implemented on hardware.

The parity check matrix of the base rate is written as

$$\mathbf{H}_{\mathrm{BR}} = \begin{bmatrix}\mathbf{H}_{\mathrm{d}} & \mathbf{H}_{\mathrm{p}}\end{bmatrix}, \tag{7}$$

Here, such a base rate has the code rate of $\frac{k}{n_{\mathrm{BR}}}$. The lower-rate parity check matrices are extended versions of the base parity check matrix by the same number of rows and columns. Let denote $\mathbf{H}^{(i)}$ as an extended version of the base parity check matrix by i rows and columns $(0 \le i \le n_{\mathrm{IR}})$, which can be expressed as

$$\mathbf{H}^{(i)} = \begin{bmatrix}\mathbf{H}_{\mathrm{BR}} & \mathbf{0} \\ \mathbf{H}_{\mathrm{IR}}^{(i)} & \mathbf{I}\end{bmatrix}, \tag{8}$$

where $\mathbf{H}_{\mathrm{IR}}^{(i)}$ is the first i rows of $\mathbf{H}_{\mathrm{IR}}$. The matrix $\mathbf{H}^{(i)}$ has the size of $(m_{\mathrm{BR}}+i) \times (n_{\mathrm{BR}}+i)$ and code rate of $\frac{k}{n_{\mathrm{BR}}+i}$. It can be seen that the extended matrix has a lower rate yet the same information bits compared to the base parity check matrix. In addition, the possible code rates of the family range from $\frac{k}{n_{\mathrm{BR}}}$ to $\frac{k}{n_{\mathrm{BR}}+n_{\mathrm{IR}}}$.

For systematic encoding, we denote the systematic generator matrix for the base code rate as

$$\mathbf{G}_{\mathrm{BR}} = \begin{bmatrix}\mathbf{I} & \mathbf{H}_{\mathrm{d}}^{\mathrm{T}}\mathbf{H}_{\mathrm{p}}^{-\mathrm{T}}\end{bmatrix}. \tag{9}$$

In this case, we assume that $\mathbf{H}_{\mathrm{p}}$ has full rank. Since $\mathbf{H}_{\mathrm{p}}$ is a square matrix, it is invertible, and there exists $\mathbf{H}_{\mathrm{p}}^{-\mathrm{T}}$. The decoding methods in case of rank deficient $\mathbf{H}_{\mathrm{p}}$ can be found on [14]. For the code rate $\frac{k}{n_{\mathrm{BR}}+i}$ with the parity check matrix $\mathbf{H}^{(i)}$, it can be considered as a concatenated code where the outer code is the base code, and the inner code is a block code whose generator matrix is

$$\mathbf{G}_{\mathrm{IR}}^{(i)} = \begin{bmatrix}\mathbf{I} & \left(\mathbf{H}_{\mathrm{IR}}^{(i)}\right)^{\mathrm{T}}\end{bmatrix}. \tag{10}$$

Thus, for a given k information bits denoted as vector $\mathbf{m}$, the LDPC-coded frame at rate $\frac{k}{n_{\mathrm{BR}}+i}$ can be computed as

$$\mathbf{c}^{(i)} = \mathbf{m}\mathbf{G}_{\mathrm{BR}}\mathbf{G}_{\mathrm{IR}}^{(i)} = \mathbf{c}^{(0)}\mathbf{G}_{\mathrm{IR}}^{(i)}, \tag{11}$$

where $\mathbf{c}^{(0)} = \mathbf{m}\mathbf{G}_{\mathrm{BR}}$ is the coded frame of the base rate. It can be seen that the frame of an arbitrary rate in the family is always systematic and nested in lower-rate frames. Therefore, we can construct low-rate frames by appending additional parity bits to a higher-rate one.

B. IR-HARQ-based LDPC with Burst Transmission

Let denote all the code rates of the RC-LDPC family as $C_1 > C_2 > ... > C_M$, where M represents both the number of code rates and the maximum number of transmissions. If $C_1 = 1$, the first transmission is an uncoded frame; otherwise, it is an LDPC-coded frame of rate C_1. On the receiver side, we assume that the iterative BP algorithm is employed for

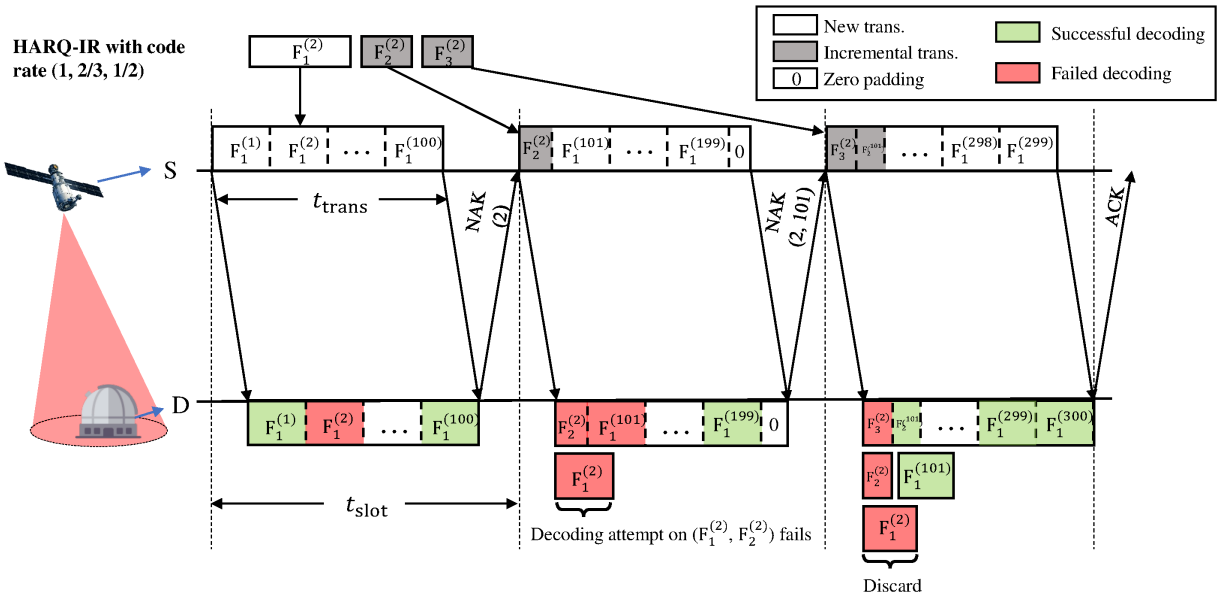

Fig. 3. An example of the IR-HARQ-based RC-LDPC code extension with burst transmission.

decoding received frames [15]. For OOK modulation, the log-likelihood ratio of j-th bit in codeword, c_j, is computed as

$$\text{LLR}\left(c_j\right) = \log \frac{\Pr\left(y_j|x_1\right)}{\Pr\left(y_j|x_0\right)} = \frac{2P_{\text{t}}\left(h^2 - hy_j\right)}{\sigma_{\text{n}}^2}. \tag{12}$$

If the decoding attempt for a frame fails after a predefined number of iterations, the frame is considered to be erroneous. The transmitter then includes the incremental transmissions of these erroneous frames in the next burst. These incremental transmissions contain redundancy that can be appended to previously received frames and form a new lower-rate frame $(C_2, ..., C_M)$. The transmission procedure stops if a decoding attempt is successful, or the frame reaches the maximum number of transmissions. For the latter case, the system then discards the frame.

Fig. 3 describes an example of the LDPC-based IR-HARQ applied in the desired system. The RC-LDPC code rates are $(1, 2/3, 1/2)$. It is observed that (1) the maximum number of transmissions is 3; (2) the second and third transmissions are redundancies whose length is half of the initial transmission; (3) the burst size allows for a maximum number of 100 new transmission frames. For the first burst, the initial transmission of the second frame denoted as $\text{F}_1^{(2)}$ is corrupted, and a NAK(2) is sent back accordingly. The transmitter then sends the redundancy $\text{F}_2^{(2)}$ in the second burst so it can combine with $\text{F}_1^{(2)}$ to form a new frame of rate 2/3 at the receiver. After the third burst, frame 2 reaches the maximum number of transmissions and is still uncorrectable. Therefore, the system discards frame 2.

IV. Simulation Results

This section presents and discusses the performance of IR-HARQ-based LDPC code extension using Monte Carlo simulations. Performance metrics, including goodput and energy efficiency, are considered. Here, the goodput is defined as the average number of successfully transmitted information bits per burst transmission. Additionally, the energy efficiency represents the successfully transmitted data bits per joule and can be calculated as the ratio between the goodput and the transmitted power.

TABLE I
System Parameters

Name	Symbol	Value
LEO Satellite Parameters		
LEO satellite altitude	H_{s}	600 km
Zenith angle	ξ	60°
Divergence half-angle	θ	10 μrad
Bit rate	R_{b}	1 Gbps
Number of bits per burst	N_{burst}	1.6 Mbits
Optical wavelength	λ	1550 nm
Ground Station Parameters		
Ground station altitude	H_{r}	1.5 m
Aperture radius	r_{a}	5 cm
Radial displacement	ρ	0 m
Noise standard deviation	σ_{n}	10^{-7} A/Hz
Detector responsivity	$\mathfrak{R}$	0.9
Other Parameters		
Atmospheric altitude	H_{a}	20 km
Rms wind speed	w_{wind}	21 m/s
Ground turbulence level	$C_n^2\,(0)$	10^{-14} m$^{-2/3}$
Visibility	V	20 km

For the simulations, we consider two sets of RC-LDPC code family, i.e. $(1, 1/2, 1/3)$ and $(1, 2/3, 1/2)$. The parity check matrix of these families is constructed by lifting a protograph two times, where the second lifting uses the circulant progressive edge growth algorithm [16]. The protograph is found

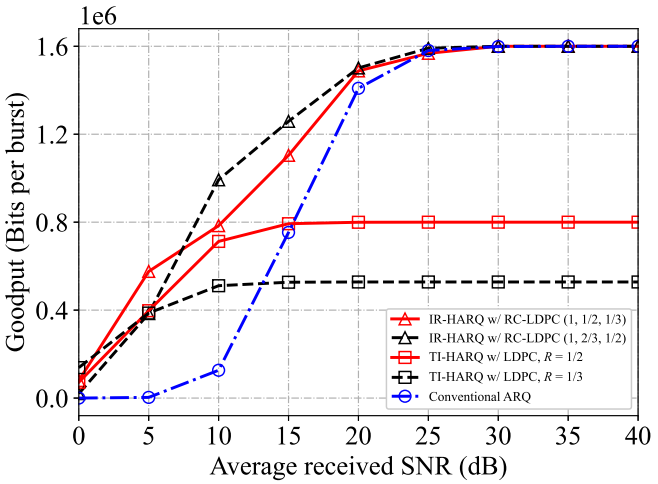

Fig. 4. Goodput versus average received SNR for different retransmission-based schemes.

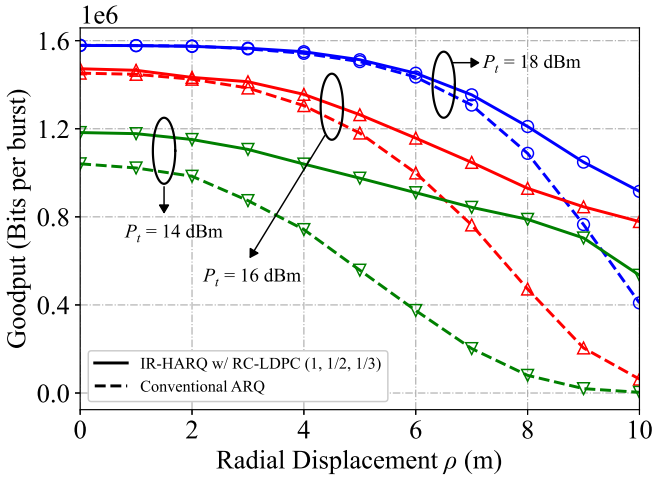

Fig. 5. Goodput versus radial displacements for different transmitted power values.

in [11, (13, 14)]. The first and second lifting factors are 4 and 250, giving the information bits of 8000. The maximum number of iterations for the BP decoder is 20. We consider a collimated beam with $F_0 = \infty$. The maximum number of transmissions M is 3. Other system parameters can be found in Table I unless otherwise stated.

Firstly, we investigate in Fig. 4 the goodput performance for different retransmission-based schemes, i.e., the IR-HARQ-based LDPC code extension, type I (TI)-HARQ, and pure sliding window ARQ protocols. As seen, the IR-HARQ-based LDPC code extension outperforms the conventional solutions of TI-HARQ and pure ARQ thanks to the retransmission of only incremental redundancies for erroneous frames. For instance, to maintain the goodput of 0.8 Mbits/burst, our proposed solution can achieve 7 dB of SNR gain compared to the pure ARQ protocols. While TI-HARQ, which contains the same LDPC-coded frame for each transmission, performs better than the ARQ in the low SNR regime (0-10 dB), its maximum achievable goodput is bounded due to the fixed code rate. In addition, the goodput of the IR-HARQ with the RC-LDPC family $(1, 2/3, 1/2)$ shows a better performance than the one with the RC-LDPC family $(1, 1/2, 1/3)$ in the SNR range of 10 to 20 dB. This is because the RC-LDPC code family $(1, 2/3, 1/2)$ has less redundancies in the incremental transmissions, which contain more new frame transmissions in the same burst.

Next, Fig. 5 illustrates the advantages of the IR-HARQ-based LDPC code extension over the conventional ARQ regarding radial displacement. Also, different transmitted power values, i.e., P_{t} = 14 dBm, 16 dBm, and 18 dBm, are taken into account. This is an especially essential performance metric to determine the operational coverage area of LEO satellite-based FSO systems. Using this figure, we can determine the operational area of the receiver to maintain a targeted goodput. For example, to maintain a targeted IR-HARQ's goodput of 1 Mb/burst, the receiver should be placed at 4 m, 7 m, and 10 m from the center of the beam footprint when P_{t} = 14 dBm, 16 dBm, and 18 dBm, respectively.

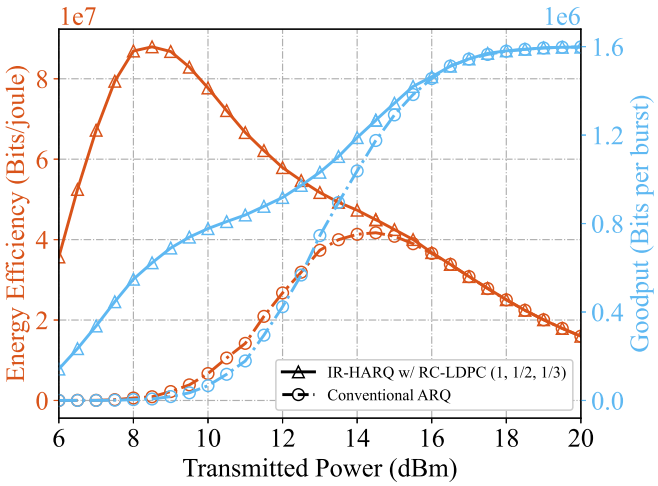

Fig. 6. Energy efficiency and goodput versus transmitted power for LDPC-based IR-HARQ and conventional ARQ.

Finally, we explore the tradeoff between energy efficiency and the goodput over a range of transmitted powers in Fig. 6. Also, both IR-HARQ-based LDPC code extension and pure sliding window ARQ protocols are considered. As expected, our proposed solution outperforms the conventional ARQ in terms of energy efficiency. Using this figure, we can determine a proper transmitted power to maximize the system's energy efficiency while maintaining a required level of goodput performance. For instance, to retain a required IR-HARQ's goodput level of 0.8 Mb/burst while achieving the optimal value of energy efficiency, the transmitted power should be 10 dBm.

V. Conclusion

In this paper, we have presented the design and performance evaluation of the IR-HARQ-based RC-LDPC code extension for LEO satellite-based FSO systems. To facilitate the operation of IR-HARQ, we used the RC-LDPC code family derived by code extension for incremental redundancy retransmission. Performance metrics, i.e., goodput and energy efficiency, were investigated. The simulation results highlighted the outperformance of IR-HARQ-based LDPC code extension compared to the conventional solutions, i.e., TI-HARQ and pure sliding window ARQ protocols. Furthermore, the results also explored the trade-off between goodput and energy efficiency, which supports the proper selection of transmitted powers.

References

[1] D. C. Nguyen, M. Ding, P. N. Pathirana, A. Seneviratne, J. Li, D. Niyato, O. Dobre, and H. V. Poor, "6g internet of things: A comprehensive survey," *IEEE Internet Things J.*, vol. 9, no. 1, pp. 359–383, 2021.

[2] H. D. Le, H. D. Nguyen, C. T. Nguyen, and A. T. Pham, "Fso-based space-air-ground integrated vehicular networks: Cooperative harq with rate adaptation," *IEEE Trans. Aerosp. Electron. Syst.*, 2023.

[3] H. D. Le, P. V. Trinh, T. V. Pham, D. R. Kolev, A. Carrasco-Casado, T. Kubo-Oka, M. Toyoshima, and A. T. Pham, "Throughput analysis for tcp over the fso-based satellite-assisted internet of vehicles," *IEEE Trans. Veh. Technol.*, vol. 71, no. 2, pp. 1875–1890, 2021.

[4] H. D. Le and A. T. Pham, "Level crossing rate and average fade duration of satellite-to-uav fso channels," *IEEE Photon. J.*, vol. 13, no. 1, pp. 1–14, Feb. 2021.

[5] J. Ma, K. Li, L. Tan, S. Yu, and Y. Cao, "Performance analysis of satellite-to-ground downlink coherent optical communications with spatial diversity over gamma–gamma atmospheric turbulence," *Appl. Opt.*, vol. 54, no. 25, pp. 7575–7585, Aug. 2015.

[6] H. D. Le and A. T. Pham, "On the design of fso-based satellite systems using incremental redundancy hybrid arq protocols with rate adaptation," *IEEE Trans. Veh.*, vol. 71, no. 1, pp. 463–477, Nov. 2021.

[7] H. D. Nguyen, H. D. Le, C. T. Nguyen, and A. T. Pham, "Throughput and delay performance of cooperative harq in satellite-hap-vehicle fso systems," in *Proc. IEEE Veh. Technol. Conf*, Norman, OK, USA, Sept. 2021, pp. 1–6.

[8] T. T. Kapsis and A. D. Panagopoulos, "Power allocation for reliable and energy-efficient optical leo-to-ground downlinks with hybrid arq schemes," in *MDPI Photonics*, vol. 9, no. 2, Feb. 2022, p. 92.

[9] J. Luo, "On low-complexity maximum-likelihood decoding of convolutional codes," *IEEE Trans. Inf.*, vol. 54, no. 12, pp. 5756–5760, 2008.

[10] T. Buerner, R. Dohmen, A. Zottmann, M. Saeger, and A. van Wijngaarden, "On a high-speed reed-solomon codec architecture for 43 gb/s optical transmission systems," in *Proc. 24th Int. Conf. Microelectron*, vol. 2. IEEE, 2004, pp. 743–746.

[11] T.-Y. Chen, K. Vakilinia, D. Divsalar, and R. D. Wesel, "Protograph-based raptor-like ldpc codes," *IEEE Trans. Commun.*, vol. 63, no. 5, pp. 1522–1532, Feb. 2015.

[12] A. A. Farid and S. Hranilovic, "Outage capacity optimization for free-space optical links with pointing errors," *IEEE/OSA J. Lightwave Technol.*, vol. 25, no. 7, pp. 1702–1710, July 2007.

[13] L. Andrews, R. Phillips, and P. Yu, "Optical scintillations and fade statistics for a satellite-communication system," *OSA Appl. Opt.*, vol. 34, no. 33, pp. 7742–7751, Nov. 1995.

[14] Z. Li, L. Chen, L. Zeng, S. Lin, and W. H. Fong, "Efficient encoding of quasi-cyclic low-density parity-check codes," *IEEE Trans. Commun.*, vol. 54, no. 1, pp. 71–81, Jan. 2006.

[15] T. J. Richardson and R. L. Urbanke, "The capacity of low-density parity-check codes under message-passing decoding," *IEEE Trans. Inf. Theory*, vol. 47, no. 2, pp. 599–618, Feb. 2001.

[16] Z. Li and B. V. Kumar, "A class of good quasi-cyclic low-density parity check codes based on progressive edge growth graph," in *Conf. Rec. 38th Asilomar Conf. Signals, Syst. Comput*, vol. 2, Pacific Grove, CA, USA, 2004, pp. 1990–1994.